Available online at www.sciencedirect.com
ScienceDirect
Fusion Engineering and Design 82 (2007) 1607–1613
Fusion Engineering and Design
www.elsevier.com/locate/fusengdes

Multi-solid multi-channel Mithrandir (M^3) code for thermal–hydraulic modelling of ITER Cable-in-Conduit Superconductors

L. Savoldi Richard, M. Bagnasco, R. Zanino *

Dipartimento di Energetica, Politecnico, C.so Duca degli abruzzi 24, 10129 Torino, Italy

Received 31 July 2006; accepted 19 April 2007
Available online 11 June 2007

Abstract

We present a new multi-solid multi-channel (M^3) thermal–hydraulic model for the analysis of the International Thermonuclear Experimental Reactor (ITER) Cable-In-Conduit Conductors (CICC). The model discretizes the cross section of an ITER CICC into M current carrying cable elements (e.g., the six last-but-one cabling stages—the petals), coupled with N hydraulic channels (e.g., the six petals + the central channel) and K non-current carrying solid components (e.g., the jacket of the CICC), with M, N and K arbitrary integers. Along each of the M + K solid components a 1D transient heat conduction equation is solved, whereas along each of the N channels three Euler-like 1D equations, derived from the conservation laws for compressible He flow, are solved. The resulting quasi 3D model, in which 1D equations are coupled by heat and mass transfer between the different CICC components, is implemented in the M^3 code and validated against experimental results from the ITER Good Joint sample and the ITER Poloidal Field Conductor Insert Full Size Joint Sample. The new code is able to reproduce with good accuracy the measured temperature gradients *on the CICC cross section*, provided sufficiently accurate input data are available.

Keywords: ITER; CICC; Thermal–hydraulic transients

1. Introduction

The superconducting magnets of the International Thermonuclear Experimental Reactor (ITER) will be wound using Cable-In-Conduit Conductors (CICC). Because of the multi-stage and multi-channel structure of the ITER CICC, the analysis of thermal–hydraulic transients requires sophisticated computational tools. Most of the present validated codes, like Mithrandir [1], M&M [2] and THELMA [3], assume on each cross section a uniform temperature for the superconducting strands and a uniform (typically different) temperature for the helium in the annular (cable) region. However, tests of short full-size ITER CICC samples in the SULTAN facility at Villigen PSI, Switzerland, have shown

* Corresponding author. Tel.: +39 011 564 4490.
E-mail address: roberto.zanino@polito.it (R. Zanino).

0920-3796/$ – see front matter © 2007 Elsevier B.V. All rights reserved.
doi:10.1016/j.fusengdes.2007.04.035

that azimuthal temperature gradients arise under particular external heating conditions. The test of two of those samples is particularly relevant here: the Good Joint (GJ) sample in 1999 [4], and the Poloidal Field Conductor Insert Full Size Joint Sample (PFCI-FSJS) in 2004 [5]. During those tests, the presence of temperature gradients in the bundle region of the full-size conductors was revealed by so-called local heaters, combined with an adequate positioning of the temperature sensors.

Furthermore and perhaps more importantly, local temperature non-uniformities may arise in the annular region also because of intrinsic reasons, e.g., the local overheating of a single strand reaching current sharing as first cable element in the CICC [6]. Indirect evidence for the latter type of phenomena comes, e.g., from the so-called "sudden quench" in NbTi conductors, which has been so far explained (but only qualitatively) as the combined effect of magnetic field and thermal gradients on the conductor cross section, coupled to a possible current non uniformity [5].

It is therefore essential to extend the modelling capabilities of the Mithrandir code, moving in some sense from a 1D to a quasi-3D model of the CICC thermal–hydraulics. The same model will be implemented in the thermal–hydraulic module of the THELMA code [7].

Here, we present a multi-solid multi-channel model for the analysis of thermal–hydraulic transients in ITER-relevant CICC, and we apply the new tool to the simulation of transients in a CICC driven by local heaters, which can heat selectively only a portion of the cable annular region. Although other multi-solid multi-channel models have already been presented in [8,9], this is, to the best of our knowledge, the first time that such a model is used to reproduce the measured temperature evolution during heating tests of full-size ITER CICC, with the evidence of temperature non-uniformity on the cable cross section.

2. Multi-solid multi-channel model

The Multi-solid Multi-channel Mithrandir (M^3) model describes the thermal–hydraulic transients on superconducting cables, which consist of:

- N channels with supercritical helium (SHe) forced-convection flow (subscript i).
- M current-carrying solids, also called Cable Elements (CE), which may go from the strand to the whole cable level (subscript j).
- K other (non current-carrying) solids, like jacket, central spiral, wrappings, ... (subscript k).

This extends significantly the capabilities of the model with respect to its parent, the Mithrandir code [1], wherein $N=2$, $M=1$ and $K=1$ were hardwired. While a similar structure is also adopted in [8], the number of channels in [9] is fixed by the number of CEs, since in that model each CE is surrounded by two layers of helium. Therefore, the model in [9] introduces artificial boundaries between hydraulic channels, which increase the number of unknown (free) parameters of the simulations.

For each He channel a set of Euler-like fluid equations in the non-conservative (primitive) variables speed (v), pressure (p) and temperature (T) is solved, derived from mass, momentum and energy conservation laws:

$$\begin{cases} \dfrac{\partial v_i}{\partial t} + v_i \dfrac{\partial v_i}{\partial x} + \dfrac{1}{\rho_i}\dfrac{\partial p_i}{\partial x} = \dfrac{1}{\rho_i}[\Lambda_{v,i} - v_i \Lambda_{\rho,i}] \\ \dfrac{\partial p_i}{\partial t} + v_i \dfrac{\partial p_i}{\partial x} + \rho_i c^2 \dfrac{\partial v_i}{\partial x} + \Phi_i \rho_i v_i g \cos\beta = \Phi_i \left[\Lambda_{e,i} - v_i \Lambda_{v,i} - \left(w_i - \dfrac{v_i^2}{2} - \dfrac{c^2}{\Phi_i} + g z_i \right) \Lambda_{\rho,i} \right] \\ \dfrac{\partial T_i}{\partial t} + v_i \dfrac{\partial T_i}{\partial x} + \Phi_i T_i \dfrac{\partial v_i}{\partial x} + \dfrac{1}{C_{v,i}} v_i g \cos\beta = \dfrac{1}{\rho_i C_{v,i}} \left[\Lambda_{e,i} - v_i \Lambda_{v,i} - \left(w_i - \dfrac{v_i^2}{2} - \Phi_i C_{v,i} T_i + g z_i \right) \Lambda_{\rho,i} \right] \end{cases} \quad (1.1)$$

where c is the sound speed, Φ is the Gruneisen parameter, w is the He enthalpy, z is the height, C_v is the specific heat at constant volume, g is the gravity acceleration, β is the angle between the vertical (upwards) direction and the flow direction and the Λ terms represent the sources in the mass (subscript ρ), momentum (subscript v) and energy (subscript e) equations, respectively,

including both advective and conductive contributions to the transverse fluxes between different cable components. As, to the best of our knowledge, no validated models are presently available for either contribution, we assume here that the *advective* fluxes are driven by the pressure difference between two neighboring He channels, as in [1], while the *conductive* fluxes are driven by the temperature difference, again as in [1]. Λ_e includes also the thermal coupling between He and solid components. Small differences are present in Eq. (1.1) with respect to the model in [8], concerning the contribution of the gravity term, here accounted for, and the contribution of cross section variations along the channels that is neglected here.

The temperature of each CE is modeled by the transient 1D heat equation

$$A_j \rho_j C_j \frac{\partial T_j}{\partial t} + A_j \frac{\partial}{\partial x}\left(k_j \frac{\partial T_j}{\partial x}\right) = \Gamma_{\mathrm{He},j} + \Gamma_{\mathrm{St},j} + \Gamma_{\mathrm{Jk},j} + Q_{\mathrm{Joule},j} + Q_{\mathrm{ext},j} \quad (1.2)$$

where A_j is the CE transverse area, ρ_j the CE density, weighed on the different components, C_j the CE specific heat, weighed on the different components, k_j the CE thermal conductivity, weighed on the different components, $\Gamma_{\mathrm{He},j}$ accounts for the heat transfer between He channels and the j-th CE, $\Gamma_{\mathrm{St},j}$ accounts for the heat transfer between the CE's and the j-th CE, $\Gamma_{\mathrm{Jk},j}$ accounts for the heat transfer between the other solids and the j-th CE, Q_{Joule} is the Joule linear power (W/m) generated in the CE and $Q_{\mathrm{ext},j}$ is the external linear power going into the CE.

The remaining K solids are also modelled by means of Eq. (1.2) with $Q_{\mathrm{Joule}} = 0$, as they carry no current in the model.

The coupling between the different components (CE–CE, CE–channel, channel–channel, solid–solid, solid–CE, solid–channel) is defined in input by means of a coupling matrix. The final set of equations, containing $3 \times N + M + K$ equations, is discretized and solved on a fixed mesh as described in [1,2], resulting in the *implicit* coupling among all components.

3. The Good Joint (GJ) sample local heater tests

The GJ sample consists of two full-size CICC's, cooled from bottom to top with SHe at ~1 MPa and 4.5 K. The main conductor data are reported in [4]. A local heater (active area ~24 mm azimuthal × 126 mm axial) was mounted on one leg for calorimetric calibration purposes, but it turned out to be also useful in verifying the speculation on the presence of a non-homogeneous temperature in the bundle region [4]. An additional temperature sensor (*T*4, see Fig. 1a) was installed for that purpose on the conductor ~250 mm (i.e., about half a petal pitch) downstream of the end of the heater, rotated azimuthally by 180° with respect to the temperature sensor *T*6. All the above-mentioned temperature sensors measure directly the SHe temperature. Finally, the central channel in these tests was blocked with a rubber pipe.

The tests were performed at different mass flow rates using the local heater, increasing the heating power in steps, showing that a temperature difference >0.5 K could arise in the conductor, for a heating power ~6.3 W and with mass flow rate ~6.8 g/s.

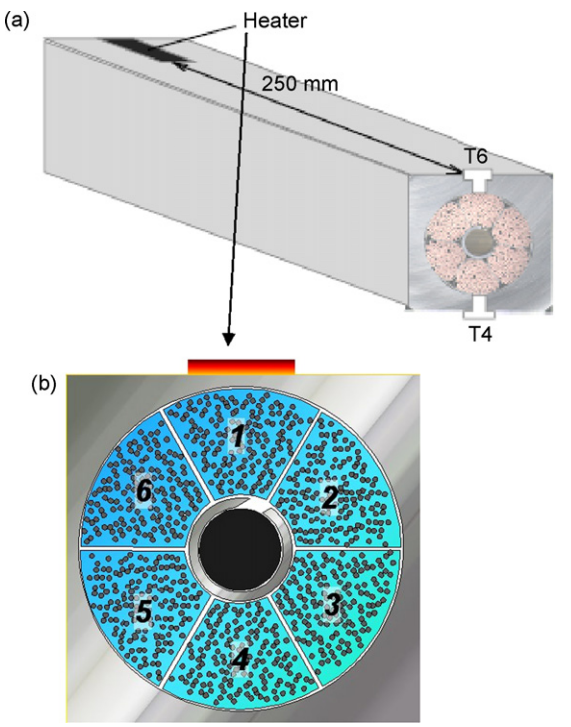

Fig. 1. (a) Sketch of the layout of the local heater and temperature sensors on one GJ leg (taken from [4]). (b) Sketch of a possible CE position on the conductor cross section at the beginning of the heater region in the GJ test.

3.1. M^3 model

The heating of one leg of the GJ conductor by the local heater is a fully 3D problem, which we try here to simplify in order to apply the M^3 code. The simulation of the local heater tests of the GJ sample was already attempted with the M&M code [2], modeling each petal as a conductor (without central channel), and accounting explicitly for the mass and energy transfer between the different conductors [10]. That exercise gave a qualitative agreement with the experimental results; moreover, the coupling between the different cable components was treated in *explicit* and this turned out to be a limiting factor in the simulations, in view of the strong thermal–hydraulic coupling among the petals.

In order to simulate the local heater tests with the M^3 code, we model six CEs, each coupled with its hydraulic channel – thus reproducing the petal structure of the conductor, see Fig. 1b, and a single jacket (under the assumption that the blocked central channel is adiabatic, i.e., neglecting the heat capacity of the spiral delimiting the central channel and of the rubber tube pulled inside). The channels are thermally coupled through a heat transfer coefficient, H_{HeHe}, which is in principle unknown and therefore used here as a free parameter, while we assume zero thermal coupling between the different CEs and between the jacket and the CEs. In principle, the petals can also exchange mass through the perforation of the petal wrapping, but this mass transfer and the associated energy transfer is neglected here in order to reduce the number of unknown parameters. We further assume that the mass flow rate splits equally among the six hydraulic channels, whereas the "triangles" between the petals and the jacket are neglected.

We assume that the deposited heat only goes into the cable, i.e., no conduction across the jacket is accounted for. Heating the jacket, as in the experiment, would allow in principle to simulate also the transient phase of the temperature evolution, but the only way to reproduce a heating affecting only a portion of the jacket with M^3 is to separately model several thermally coupled "jackets", which is feasible but rather cumbersome and possibly not very useful in view of the many other uncertainties in the problem. Therefore, in the comparison with the experimental data presented here, we will focus on the steady-state (plateau) temperatures measured at the sensors.

A realistic model of the heating should also account for the cable twisting under the heater, evaluating the fraction of the total power deposited in each petal. We assume that the local heater acts azimuthally on an angle of $\sim 60^\circ$, and that at the axial location where the heater starts, it affects mainly petal #1, see Fig. 1b. However, in view of the uncertainty on the azimuthal position of the petals under the heater, any position in the range $[-30^\circ, 30^\circ]$ around the reference one is in principle possible for the axis of petal #1. Since the petal twist pitch is an input parameter (nominal value $p = 410$ mm), the repartition of the heating power among the petals located under the heater, as well as the position of the petals in the portion of the conductor from the heater to the temperature sensors, can be computed from simple geometrical considerations. It is thus straightforward to deduce which petal is located under $T4$ and under $T6$. In this frame, the computed temperature evolution at the sensor locations will depend only on the azimuthal position of the petals under the heater and on H_{HeHe}.

3.2. Computed results

In Fig. 2a, the steady-state temperatures at $T4 - T6$ have been computed as a function of the initial azimuthal position of CE #1, with progressively increasing H_{HeHe}, for a mass flow rate of 6.8 g/s and for maximum heating power (i.e., the case with the maximum temperature difference between $T4$ and $T6$). At high $H_{\mathrm{HeHe}} = 10{,}000\ \mathrm{W/(m^2\ K)}$ the coupling among the petals is so strong that no difference is computed between $T4$ and $T6$, as expected. For values of H_{HeHe} in the range 10–1000 $\mathrm{W/(m^2\ K)}$, [1] the computed $T4$ and $T6$ are strongly influenced by the azimuthal position of the cable with respect to the heater (for $H_{\mathrm{HeHe}} < 10\ \mathrm{W/(m^2\ K)}$ the petals are basically adia-

[1] A reasonable order of magnitude for H_{HeHe} can be deduced from the analysis of the thermal-hydraulic tests of the PFCI-FSJS [11], where a global heat transfer coefficient H of ~ 150–$250\ \mathrm{W/(m^2\ K)}$ is deduced from the analysis of the heat step propagation along the conductor at a mass flow rate of ~ 6 g/s. If the heat transfer coefficient from the hole side is much larger than that from the bundle side, a reasonable assumption in a model of series of thermal resistances, H is basically representative of the bundle heat transfer coefficient. Then, since the Reynolds number, Re, in each petal is approximately the same as the Re in the bundle, we can assume as reasonable order of magnitude of $H_{\mathrm{HeHe}} \sim 100\ \mathrm{W/(m^2\ K)}$.

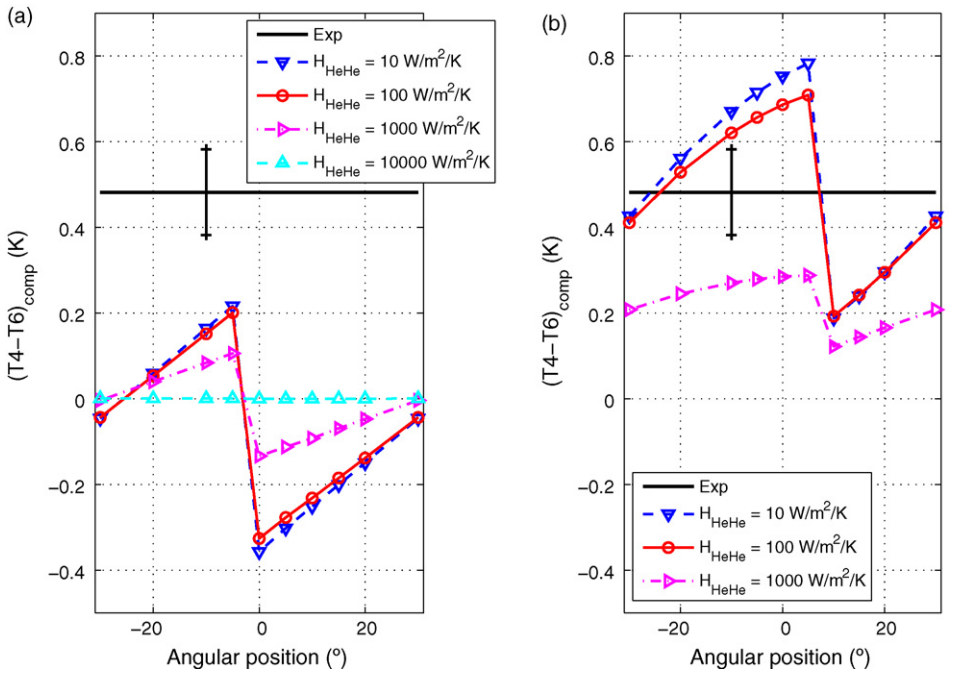

Fig. 2. Temperature difference $T4 - T6$ as a function of the azimuthal position of the CE 1 in the conductor cross section where the heater begins, computed using different values of the heat transfer coefficient H_{HeHe} (a) with petal twist pitch $p = 410$ mm and (b) with $p = 520$ mm. The experimental value is also reported, with its errorbar.

batic). The change in sign of $(T4 - T6)_{\mathrm{comp}}$ is due to the switch of CE under the temperature sensors. The maximum computed difference $(T4 - T6)_{\mathrm{comp}}$ is ∼0.2 K, which is much lower than the measured value, suggesting that with the nominal petal twist pitch $p = 410$ mm one does not succeed in reproducing the measured temperature increase, whatever the coupling parameters and the rotation of the cable under the heater are.

During the sample manufacturing, indeed, it turned out that the actual pitch of the last-but-one cabling stage was ∼520−550 mm [4]. The computed $(T4 - T6)$ is reported in Fig. 2b as a function of the initial azimuthal position of petal #1, for the case $p = 520$ mm. Now the computed value of $(T4 - T6)$ well reproduces the experimental one, within its error bar, for a wide range of azimuthal positions of CE #1 and realistic values of H_{HeHe}, see above.

4. The PFCI-FSJS local heater tests

Also the PFCI-FSJS consists of two short full-size CICC's (legs) [5]. A local heater (active area ∼5 mm × 20 mm) was mounted in a groove on the jacket on both legs, allowing to study the propagation of a heat slug in the conductor by means of a set of temperature sensors ($T4$, $T3$ and $T2$) mounted downstream of the heater (at 250, 400 and 600 mm distance, respectively), on a jacket face at 90° to the face where the heater is located. We study here the heat slug driven by a power of ∼ 14 W deposited for 10 s. We concentrate on the right leg where, despite the absence of petal wrappings, the temperature evolution at the sensors showed clearly the presence of non-uniformities on the cable cross section.

4.1. M^3 model and results

The cross section of the PFCI-FSJS has been modelled as in the GJ simulations, but an additional hydraulic channel was considered to account for the central channel, which was open to the flow in this case. The heat is deposited only in one CE (the petal #1 in our model) in view of the very short length of the heater, compared to the petal pitch (∼550–600 mm).

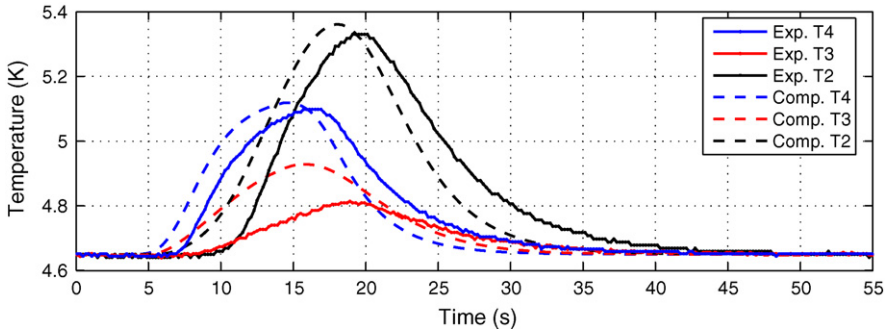

Fig. 3. Experimental (*solid*) and computed (*dashed*) temperature evolution at the sensors *T*4, *T*3 and *T*2 located along the PFCI-FSJS, during a local heater test (pulse amplitude ∼14 W, duration ∼10 s).

The free parameters of the analysis are the heat transfer coefficients between the modelled cable components: in view of the uncertainties on this point, we do not attempt here any validation, strictly speaking, but we just aim at demonstrating that there are suitable values (∼100 W/m^2K) of the heat transfer coefficients between helium and all other cable components, for which the M^3 code is able to reproduce the experimental evolution of temperature traces with good accuracy, see Fig. 3. The sensor *T*4 measures the temperature of the petal #6, which is in contact with the heated one (petal #1); the sensor *T*3 measures the temperature of the petal #4, which is the furthest from the heated one; finally, petal #1 passes by sensor *T*2. This explains why the peak in *T*2 is higher than the others, notwithstanding its location further away from the heater and confirms the strong relation between non-uniformity of the temperature on the cable cross section and petal twist. While the computed evolutions in *T*2 and *T*4 agree well with the experiment, in *T*3 the temperature is more overestimated, possibly because of accumulation of errors in the heat transfer computations. In Fig. 3 the computed traces trail the measured ones because the heat was deposited in the simulation directly in the strands. Therefore, the diffusion from the jacket to the strands cannot be accounted for.

5. Conclusions

A new quasi-3D thermal–hydraulic model for the ITER CICC has been developed and validated against experimental data from different short but full-size samples. The computed temperature gradients on the cable cross section are in good agreement with the measurements, provided, sufficiently accurate input data are available on the cable geometry. Input uncertainties like the azimuthal position of the petals with respect to the heater and/or the heat transfer coefficients between the different cable components have been dealt with parametrically, considering the sensitivity to their variation inside an acceptable range.

Besides the artificially induced temperature gradients considered here, as a result of external local heating, the model we developed will be extremely useful for the analysis of intrinsically local (on the cable cross section) heating mechanisms, like the normal transition of a single strand in a NbTi sudden quench [7].

Acknowledgments

The European Fusion Development Agreement (EFDA) and the Italian Ministry for Education, University and Research (MIUR) have partially financially supported this work.

References

[1] R. Zanino, S. De Palo, L. Bottura, A two-fluid code for the thermohydraulic transient analysis of CICC superconducting magnets, J. Fusion Energy 14 (1995) 25–40.
[2] L. Savoldi, R. Zanino, M&M: Multi-conductor Mithrandir code for the simulation of thermal–hydraulic transients in superconducting magnets, Cryogenics 40 (2000) 179–189.
[3] R. Ciotti, A. Nijhuis, P.L. Ribani, L. Savoldi Richard, R. Zanino, THELMA code electromagnetic model of ITER superconduct-

ing cables and application to the ENEA stability experiment, Supercond. Sci. and Technol. 19 (2006) 987–997.

[4] P. Bruzzone, A.M. Fuchs, G. Vecsey, E. Zapretilina, Test results of the high field conductor of the ITER central solenoid model coil, Adv. Cryo. Eng. 45 (2000) 729–736;
P. Bruzzone (Compiler), Development of an improved joint for ITER CS1 conductor and joint test in SULTAN, Villigen, December 1999.

[5] P. Bruzzone, M. Bagnasco, D. Bessette, D. Ciazynski, A. Formisano, P. Gislon, et al., Test results of the ITER PF Insert Conductor Short Sample in SULTAN, IEEE Trans. Appl. Supercond. 15 (2005) 1351–1354.

[6] R. Zanino, M. Bagnasco, W. Baker, F. Bellina, P. Bruzzone, A. della Corte, et al., Implications of NbTi short-sample test results and analysis for the ITER Poloidal Field Conductor Insert (PFCI), IEEE Trans. Appl. Supercond. 16 (2006) 886–889.

[7] R. Zanino, M. Bagnasco, L. Savoldi Richard, F. Bellina, P.L. Ribani, Multi-Solid Multi-Channel THELMA Analysis of Sudden Quench of ITER Superconducting NbTi Full-Size Short Samples, presented at CHATS06, Berkeley, California, U.S.A., September 5–7, 2006.

[8] L. Bottura, C. Rosso, M. Breschi, A general model for thermal, hydraulic and electric analysis of superconducting cables, Cryogenics 40 (2000) 617–626.

[9] N. Mitchell, Modelling of non-uniform current diffusion coupled with thermohydraulic effects in superconducting cables, Cryogenics 40 (2000) 637–653.

[10] R. Zanino, L. Savoldi, Status and perspectives of thermal–hydraulic analysis of superconducting magnets for nuclear fusion applications, IAEA-CSP-8/C CD-ROM Proceedings, IAEA, Vienna, May 2001 (Paper FTP2/01).

[11] M. Bozzola, Evaluation of the heat transfer coefficient between annulus and central channel of a superconducting cable from the analysis of experimental transients, Undergraduate Thesis, Politecnico di Torino, 2005.